Journal of Sound and Vibration 557 (2023) 117740

Contents lists available at ScienceDirect

Journal of Sound and Vibration

journal homepage: www.elsevier.com/locate/jsvi

Analysis and modelling of the dynamic stiffness up to 400 Hz of an air spring with a pipeline connected to a reservoir

I. Mendia-Garcia [a,*], A. Facchinetti [c], S. Bruni [c], N. Gil-Negrete [a,b]

[a] Universidad de Navarra, TECNUN Escuela de Ingenieria, Departament of Mechanical Engineering and Materials, Manuel Lardizabal 13, 20018 Donostia-San Sebastián, Spain

[b] CEIT-Basque Research and Technology Alliance (BRTA), Manuel Lardizabal 15, 20018, Donostia / San Sebastián, Spain, Manuel Lardizabal 15, 20018 Donostia-San Sebastián, Spain

[c] Departament of Mechanical Engineering, Politecnico di Milano, via La Masa 1, Milan 20156, Italy

ARTICLE INFO

Keywords:
Pneumatic suspension
Vibration transmission
Passive suspension
Air spring
Surge pipeline
Non-linear characteristics

ABSTRACT

The present research addresses the dynamic behaviour of an air spring with a pipeline connected to a reservoir in a frequency range up to 400 Hz, in which structure-borne vibration transmission may occur due to both the structural behaviour of the bellows and fluid dynamics in the pneumatic circuit of the suspension. Based on experimental results, three frequency ranges are distinguished where different resonances of the suspension appear: *low* (up to 30 Hz) due to the air flow between the bellows and the surge reservoir, *intermediate* (30–150 Hz) due to the formation of standing waves in the pipeline and *high* (beyond 150 Hz) due to the structural dynamics of the bellows. A novel modelling technique to predict the dynamic behaviour of the pneumatic system in all these frequency ranges is presented and validated: this consists of an enhanced Finite Element Model (FEM) considering the structural properties of the bellows and the effect of pressurised air in the bellows and in the reservoir, coupled to a model of fluid exchange between the two main air volumes which is defined using a VUFLUIDECH user subroutine developed in ABAQUS. The study focusses on the axial dynamic stiffness of the pneumatic suspension, which plays a key role in determining the transmissibility of the suspension. However, the mathematical model introduced in the paper is capable of predicting also the vibration modes of the suspension in shear and rotation, which may be relevant in some applications, e.g. when air springs are used in vehicle suspensions.

1. Introduction

Pneumatic suspensions, also known as air spring suspensions, are widely considered as an effective solution for isolating vibrations in vehicles and in industrial machinery [1–5]. A typical pneumatic suspension consists of three elements, the air spring or bellows, a surge reservoir or auxiliary chamber and a pipeline [6]. The main element is the bellows, a cavity made by fibre reinforced rubberlike elastomer. When the bellows is subjected to axial forces, the air volume in the chamber is compressed, resulting in a variation of pressure in the chamber which is propagated to the reservoir via the air inside the pipe. The increased pressure produces a decrease of the total air volume, thus providing a compliance effect. The static stiffness of the pneumatic suspension can be set to the desired value through the proper choice of the total volume of the bellows and surge reservoir. However, pneumatic suspensions

* Corresponding author.
E-mail address: imendia@tecnun.es (I. Mendia-Garcia).
URL: https://www.unav.edu/web/departamento-de-ingenieria-mecanica-y-materiales/investigacion/area-de-maquinas-y-vehiculos (I. Mendia-Garcia).

https://doi.org/10.1016/j.jsv.2023.117740
Received 17 November 2022; Received in revised form 31 March 2023; Accepted 18 April 2023
Available online 21 April 2023

Nomenclature

$\tilde{g}_i^P \tau_i$	Prony series parameters (–)
Δp	Pressure harmonic waves (Pa)
$\dot{m}$	Mass flow rate (kg s^{-1})
λ	Wavelength (m)
μ	Dynamic viscosity of the air (kg m^{-1} s^{-1})
ρ	Density of the air (kg m^{-3})
$\tilde{F}(w_0)$	Fourier transform of the force signal
$\tilde{x}(w_0)$	Fourier transform of the excitation signal
$_0$	Subscript for the air spring reference state
$_b$	Subscript for the air spring or bellows
$_h$	Subscript for the high frequency range
$_i$	Subscript for the intermediate frequency range
$_l$	Subscript for the low frequency range
$_p$	Subscript for the pipeline
$_r$	Subscript for the reservoir
C_{10}, C_{20}, C_{30}	Coefficients of the Yeoh material model (Pa)
F	Resulting force (N)
G_0	Initial shear modulus (Pa)
G_s	Storage Modulus (Pa)
G_ℓ	Loss Modulus (Pa)
G_∞	Long-term shear modulus (Pa)
I_1	First invariant of the deviatoric strain
K	Static stiffness of the pneumatic system (N m^{-1})
k	Harmonic number (–)
K^*	Dynamic stiffness of the pneumatic system (N m^{-1})
n	Polytropic heat ratio of the air, n = 1 isothermal, n = 1,4 adiabatic (–)
p	Pressure (Pa)
p_{max}	Pressure amplitude (Pa)
R	Specific gas constant (J kg^{-1} K^{-1})
T	Temperature of the air inside the cavity (K)
t	Time (s)
U	Strain energy function
u_p	Velocity of the air inside the pipe (m s^{-1})
V	Total volume of the system (m^3)
w_k	Natural frequency (Hz)
z	Vertical displacement (m)
l_p	Loss coefficient due to singularities (–)
A_e	Effective area of the air spring (m^2)
A_m	Excitation amplitude (m)
A_p	Effective area of the pipe (m^2)
L_p	Length of the pipe (m)
w_0	Excitation frequency (rad)

exhibit a frequency dependent behaviour, due to both structural dynamics of the bellows and fluid dynamics in the air volume, which needs to be properly considered in order to ensure the satisfactory behaviour of the suspension.

Therefore, the design of pneumatic suspensions shall rely on accurate mathematical models, allowing to reproduce not only the quasi-static but also the dynamic behaviour of all suspension components in an appropriate frequency range that, depending on the application addressed, may be up to some hundred Hz. In this perspective, the prediction in the design stage of suspension resonances falling in the frequency range of interest can be decisive. It is known that at low frequencies (0-20/30 Hz), the dynamic stiffness of the pneumatic system shows a peak corresponding to a resonance of the pneumatic circuit seen as an equivalent mass-spring-damper system, with air compressibility providing the stiffness effect, viscous fluidic resistance in the pipe providing the damping term and the mass of air flowing in the pipe representing the equivalent mass of the system [7]. This phenomenon is described by both mechanical-lumped parameter models [8–11] and thermodynamic models [6,12–17] that can be found in the literature. The

value of the resonance frequency and the amplitude of the resonance peak are determined by some geometrical parameters such as the volume of the reservoir, the diameter and length of the pipeline and the area of the orifice which is often included in the pipe [1,6,11,16,18,19].

Regarding the modelling of the low frequency peak, both Berg's model [9] and Vampire model [10], which is an extension of the Nishimura model [8], include a mass representing the air inside the pipe. Alonso et al. included a variable orifice opening law which modifies the transmissibility of the suspension system to the previous mentioned mechanical models [11]. Moreover, Docquier et al. [6] compared different pipe modelling methods applied to railway pneumatic system: (a) considering the air inside the pipe as a constant moving mass and solving the motion equation, (b) expressing the air motion as a mass flow through a differential equation, (c) adopting an algebraic equation neglecting the inertia of the air, (d) introducing a fluidic resistance given by the ISO 6358 Standard and (e) as an equivalent mechanical model; they concluded that the use of the algebraic equation for short pipes can be sufficiently accurate. Quaglia and Sorli employed the fluidic resistance of ISO 6358 in a dimensionless model of the pneumatic suspension [13]; Facchinetti et al. implemented a differential equation to evaluate the ride comfort in railway vehicles [12]. Gao et al.proposed different definitions for the mass flow rate according to the inclusion of the orifice, the pipe or the orifice–pipe group for a railway suspension system [16]. Toyokufu et al. also implemented a differential equation to predict the pipeline influence in a heavy-duty bus [18]. Zhu et al. adopted the fluidic resistance model for short pipe or orifice connections and a mass flow considering the inertia for long pipes on a truck vehicle [14] and Nieto et al. developed a non-linear and linerized pneumatic system model with a restriction pipe coefficient for a 2-lobe convoluted air spring [15]. Recently, Zheng et al. describe, not only in the frequency domain (up to 20 Hz) but also in the time domain, the performance of the air spring with the reservoir connected with a pipeline or orifice by means of transmitted force response models with different excitation signals [17]. They also try to give a further explanation of the physical origin of this resonance by means of simulating the displacement and flow of the air in the pipeline, and conclude that they are excited when the excitation frequency is close to the natural frequency of the pipe [20].

All the above mentioned studies are focused on the performance of the pneumatic system in a frequency range up to 20–30 Hz, whilst a constant value of the dynamic stiffness is assumed for the suspension at higher frequencies, under the assumption that fluid exchange between the bellows and the surge reservoir becomes negligible above this frequency and that the effect of structural resonances in the bellows can be neglected [6,18].

Only few references address the dynamic behaviour of pneumatic suspensions at frequencies beyond 20 Hz, but they just consider the effect of structural vibration modes of the air spring [21–23] whilst high-frequency effects in the pneumatic circuit are neglected. Furthermore, only two references present experimental results for a pneumatic suspension excited at frequencies higher than few tens of Hertz [21,23]. The study of structural vibration of the bellows is based on Finite Element models combined with modal analysis. Single lobe convoluted air springs show vibration modes below 400 Hz [21,22] whilst structural resonances of rolling lobe air springs for railway applications are found below 200 Hz [23].

Nowadays, the latest research conducted in air spring pneumatic systems tends to include and explain the non-linear dynamic behaviour up to 20 Hz [20,24,25], highlighting the influence of bellows' rubberlike material and of the connecting element between the air spring and reservoir in the axial response of the air spring. Up to date, even if the dependency of excitation amplitude in the first resonant peak was observed [11], the non-linear behaviour of the material was included in the models considering the shear behaviour of the air spring, but not in models addressing the axial forces in the suspension [9,10].

The aim of this paper is to investigate the behaviour of a pneumatic suspension in a frequency range up to 400 Hz and provide a physical explanation for the observable phenomena, analysing the interaction between structural vibration of the bellows and pressure waves in the pneumatic circuit of the suspension. To this aim, laboratory tests are performed on a small-size single convoluted air spring widely used for vibration isolation in industrial machinery. A mathematical model is proposed, consisting of an enhanced finite element model developed in ABAQUS, which considers the non-linear elasticity and frequency-dependent behaviour of the rubberlike material of the bellows, and, at the same time, models the thermodynamic processes in the air contained in the bellows, reservoir and pipe. Furthermore, the presence of air spring resonances found from the experiments in an intermediate frequency range from 30 to 150 Hz is explained based on the features of the standing waves of air pressure variation taking place in the pipe.

The paper is organised as follows: in Section 2 the experimental set-up is described and the results of tests are presented. Section 3 presents the enhanced FE model. In Section 4 the results of the proposed model are presented and compared to the experimental results. Finally, Section 5 provides the conclusions of this research.

2. Experimental characterisation of the air suspension

The objective of this section is to describe the experimental tests performed to characterise the dynamic behaviour of a pneumatic suspension system, and their results.

2.1. Experimental setup

The dynamic behaviour of a pneumatic system is investigated experimentally in the 0–400 Hz frequency range. To this aim, a convoluted air spring (FS 40-6 CI manufactured by Contitech), widely used in machinery and tool applications, is tested using an Elastomeric-Testing System Instron MHF 25.

The test arrangement is shown in Fig. 1(a). The hydraulic testing machine includes an LVDT displacement sensor with range ±25 mm and a calibrated force sensor with range ±20 kN. A schematic representation of the pneumatic system is shown in Fig. 1(b) and

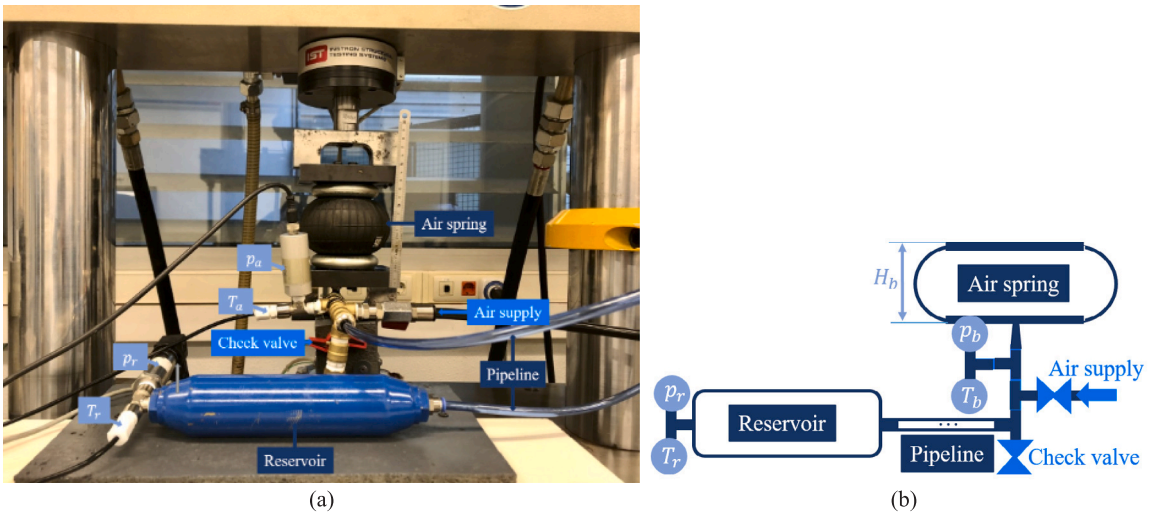

Fig. 1. Test bench layout: (a) mounting of the air spring in the testing machine, (b) pneumatic circuit and sensors layout.

Table 1
Main characteristics of the pneumatic system.

Characteristic	Value
Mounting height of the air spring (H_b)	60–100 mm
Recommended nominal height of the air spring (H_{90})	90 mm
Maximum diameter of the air spring	145 mm
Volume of the air spring (V_b)	0.5 l
Air inlet of the air spring	G 1/8
Volume of the reservoir (V_r)	0.4–1,4–4 l
Length of the pipeline (L_p)	0.5–1–2–4–8 m
Internal diameter of the pipeline (D_p)	5 mm

Fig. 2. Internal shape of the tested air spring: (a) frontal view, (b) a cut of the diaphragm of the air spring and (c) internal reinforcements of the diaphragm.

its main characteristics are summarised in Table 1. The pneumatic system is fed by a central air supply system, and a check valve is used to avoid unwanted over-pressure in the pneumatic circuit. The scheme also shows the position of two pressure transducers p_b and p_r, measuring the pressure of air respectively in the pipe close to the connection to the air spring and in the reservoir. Two companion temperature sensors (thermocouples type T), also shown in the scheme, are used to measure air temperature at the same locations. In addition, a 3D scanner is used to derive the geometrical shape of the bellows for different pressures and mounting heights. Fig. 2 depicts a photograph of a cut of the air spring diaphragm, where the rubber matrix is reinforced with two layers of single-end twisted cord yarns oriented at 60° and −60°.

Two test types are performed using the set-up: static tests and dynamic tests performed applying a swept-sine displacement at one end of the spring. Static tests are aimed to define the relationship between the applied displacement and the resulting force in quasi-static conditions when a displacement of ±5 mm is applied. Dynamic tests are instead aimed at characterising the dynamic behaviour of the pneumatic suspension. By dividing the Fourier transform of the force signal $\tilde{F}(\omega_0)$ by the Fourier transform of the

Table 2
Comparison between manufacturer data and experimental results for reaction force at working height of 90 mm and 70 mm.

90 mm mounting height			
Pressure (bar)	Manufacturer (kN)	Experimental (kN)	Deviation(%)
2	1	0.99	−1.0
3	1.5	1.46	−2.7
4	2.06	2.02	−3.8
5	2.62	2.48	−4.7
70 mm mounting height			
Pressure (bar)	Manufacturer (kN)	Experimental (kN)	Deviation (%)
2	1.4	1.4	−0.5
3	2.2	2.1	−4.5
4	2.94	2.83	−3.7
5	3.67	3.53	−3.8

excitation signal $\tilde{x}(w_0)$, both evaluated at the excitation frequency w_0, the frequency-dependent, complex-valued dynamic stiffness of the pneumatic system K^* is obtained [26]:

$$K^*(w_0) = \frac{\tilde{F}(w_0)}{\tilde{x}(w_0)}. \tag{1}$$

The real and imaginary parts of the complex-valued dynamic stiffness describe respectively the elastic and dissipative behaviour of the pneumatic suspension. As shown below, the dynamic stiffness of the pneumatic suspension is strongly affected by internal resonances of the system, so that at some frequencies known as the system's resonances a peak of the dynamic stiffness is observed, leading to a stiffer behaviour of the suspension. These internal resonances clearly affect the performance of the suspension in terms of its ability to filter out disturbance from (e.g.) a motion applied at the base. Therefore, it is extremely important not only to define experimentally these resonances, but also to obtain a physical understanding of the structural and thermodynamic phenomena producing each resonance.

2.2. Experimental results

The forces obtained from the experimental tests at different values of internal pressure and working height are compared with the values provided by the manufacturer of the air spring. The results summarised in Table 2 are found to be in good agreement, with deviations below 5% for both analysed mounting heights, 70 mm and 90 mm respectively.

In order to explore the dynamic behaviour of pneumatic suspensions at high frequencies, a sensitivity analysis has been conducted that includes, in addition to the initial pressure (P_0) and excitation amplitude (A_m), the mounting height of the air spring (H_b), the pipeline length (L_p), and the auxiliary tank volume (V_r) as factors.

Fig. 3 provides an overview of the system's dynamic behaviour in terms of the trend with frequency of the modulus (absolute value) of the dynamic stiffness over the entire frequency range from 0 Hz to 400 Hz. Fig. 3(a) shows the influence of the working pressure in the dynamics of the system; Fig. 3(b) the influence of the mounting height. Three different frequency ranges are defined for the pneumatic system, denoted as *low frequency range* (zone I up to 30 Hz), *intermediate frequency range* (zone II between 30 and 150 Hz) and *high frequency range* (zone III beyond 150 Hz).

In the *Low frequency range* a single resonance is found (see Figs. 3, 4a,b and 5a), which is related to an exchange of air between the bellows and the reservoir. This resonance is well reproduced by existing air spring models [6,10,12] and can be justified assuming the air in the pipe behaves as an incompressible fluid. As shown in Figs. 4(a) and 5(a), an increase in the length of the pipe or in the auxiliary volume increases the mass of the air volume, and hence moves the resonance to a lower frequency. The resonance amplitude is only slightly affected by the length of the pipe, whereas it is increasing with increasing reservoir volumes and with decreasing mounting heights (see 4(b)). Thus, the amplitude of this resonance peak is mainly related with the volume difference between the two cavities, the air spring and the reservoir.

In the *Intermediate frequency range*, as shown in Fig. 4(c) and (d), several resonance peaks with small amplitude are found. In regard of the number and features of these resonances, the length of the pipe plays a critical role and, in particular, the number of resonance frequencies is increasing with the length of the pipe. The mounting height and the reservoir volume can be considered as less important parameters, that slightly affect the amplitude of the resonance peaks but do not affect the resonance frequency (see Figs. 4(d) and 5(b)). This same effect was observed by Zhen et al. [20] in a lower frequency range 0–40 Hz, concerning the first peak (referred here as the low frequency peak): when the excitation frequency is close to the natural frequency of the pipe, the air displacement and then the mass flow increase rapidly, resulting in an increase in pressure followed by the rise of reaction force and of the resultant dynamic stiffness of the system, an idea that was firstly mentioned by Toyofuku et al. in 1999 [18].To the best of our knowledge, experimental evidence of resonances occurring in the *Intermediate frequency range* was not reported in the literature. The phenomena observed herein can be significant, under certain conditions, in different applications where pneumatic suspensions are implemented, such as in the secondary suspension of railway vehicles [6].

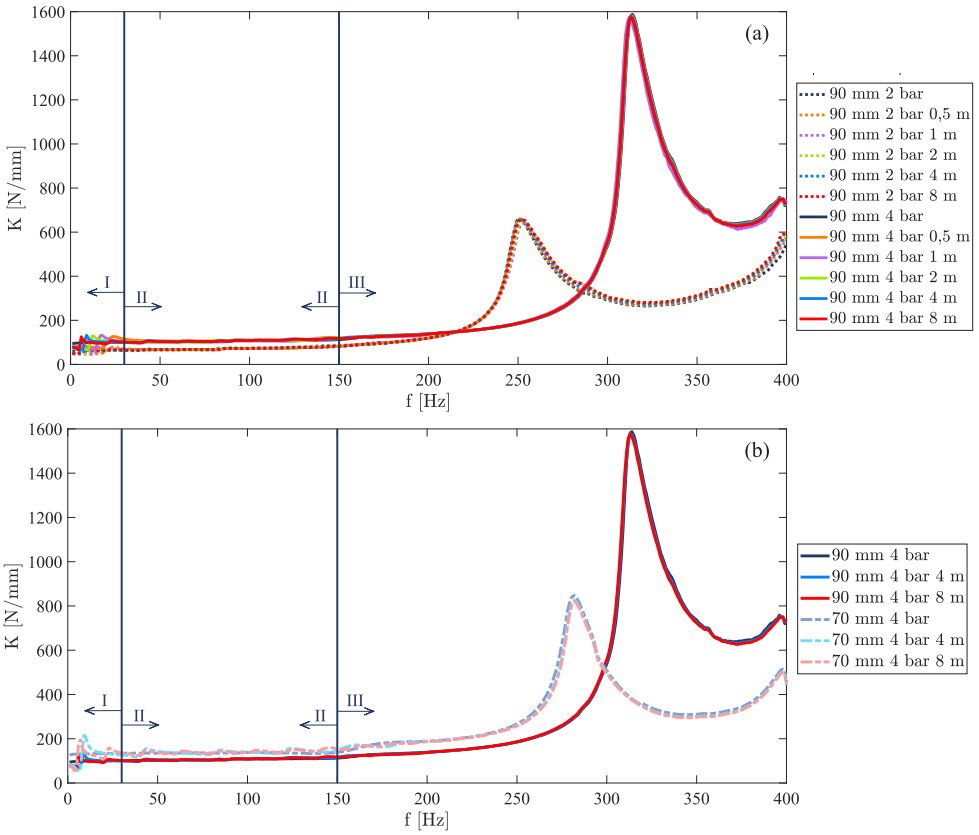

Fig. 3. Experimental FRF of the suspension system in terms of the modulus of the dynamic stiffness vs. frequency. Three frequency ranges can be distinguished: *Low* (up to 30 Hz), *Intermediate* (30–150 Hz), *High* (beyond 150 Hz). (a) for different pipe lengths (0-0.5-1-2-4-8 m) and inner pressure (2 bar and 4 bar) values mounted in the nominal height. (b) for different mounting heights (70 mm and 90 mm), pipe lengths (0-4-8 mm).

Finally, in the *high frequency range* one resonance is observed (see Figs. 3, 4e,f and 6) leading to a very large peak of the dynamic stiffness: this resonance is caused by the structural vibration of the bellows. This resonance frequency is highly affected by the internal tension in the bellows caused by air pressure, which produces a stiffening effect. Therefore, the resonance frequency increases with the air pressure, whereas it is weakly affected by the length of the pipe and by the presence of the reservoir, see Fig. 4(e). In addition, as shown in Fig. 4(d), larger mounting heights increase the value of this resonant frequency of the bellows. It is also observed (see Fig. 6) that the amplitude of excitation affects both the amplitude and frequency of the resonance peak, denoting a non-linear structural behaviour of the bellows. This non-linearity is due to the non-linear behaviour of the rubber material used to manufacture the bellows.

3. Mathematical model of the pneumatic suspension

The mathematical model of the pneumatic suspension makes use of an enhanced finite element model defined in ABAQUS complemented by a numerical model of the pipeline. The model aims to reproduce both the static and dynamic behaviour of the air spring with a pipeline connected to a reservoir.

Finite element codes allow creating an accurate model in terms of geometry and representation of the physical phenomena taking place in the system, assuming the structural properties and dimensions of the air spring system are known. For that aim, the initial shape of the flexible air spring is obtained though a 3D scanning of the bellows for different height and pressures. The generated volume is compared with the manufacturer's data. Concerning the material, the non-linear elastic and dynamic properties of the elastomeric material are experimentally obtained.

The developed FEM model should be able to include both the reinforcing fibres in the bellows and the pressurised air inside the suspension system, which plays a crucial role. Some FEM codes allow to define the air in the bellows as a fluid cavity instead of a uniform surface pressure definition. Nevertheless, even if the cavities can be modelled as fluidic ones, air dynamics is not considered in this type of model. Fluid-Structure Interaction (FSI) models are an alternative option in which fluid dynamics is considered; however, in such models the inclusion of the fibre reinforced elastomeric material of the bellows is not straightforward and it is often not supported. In addition, the computational cost and time are significantly increased.

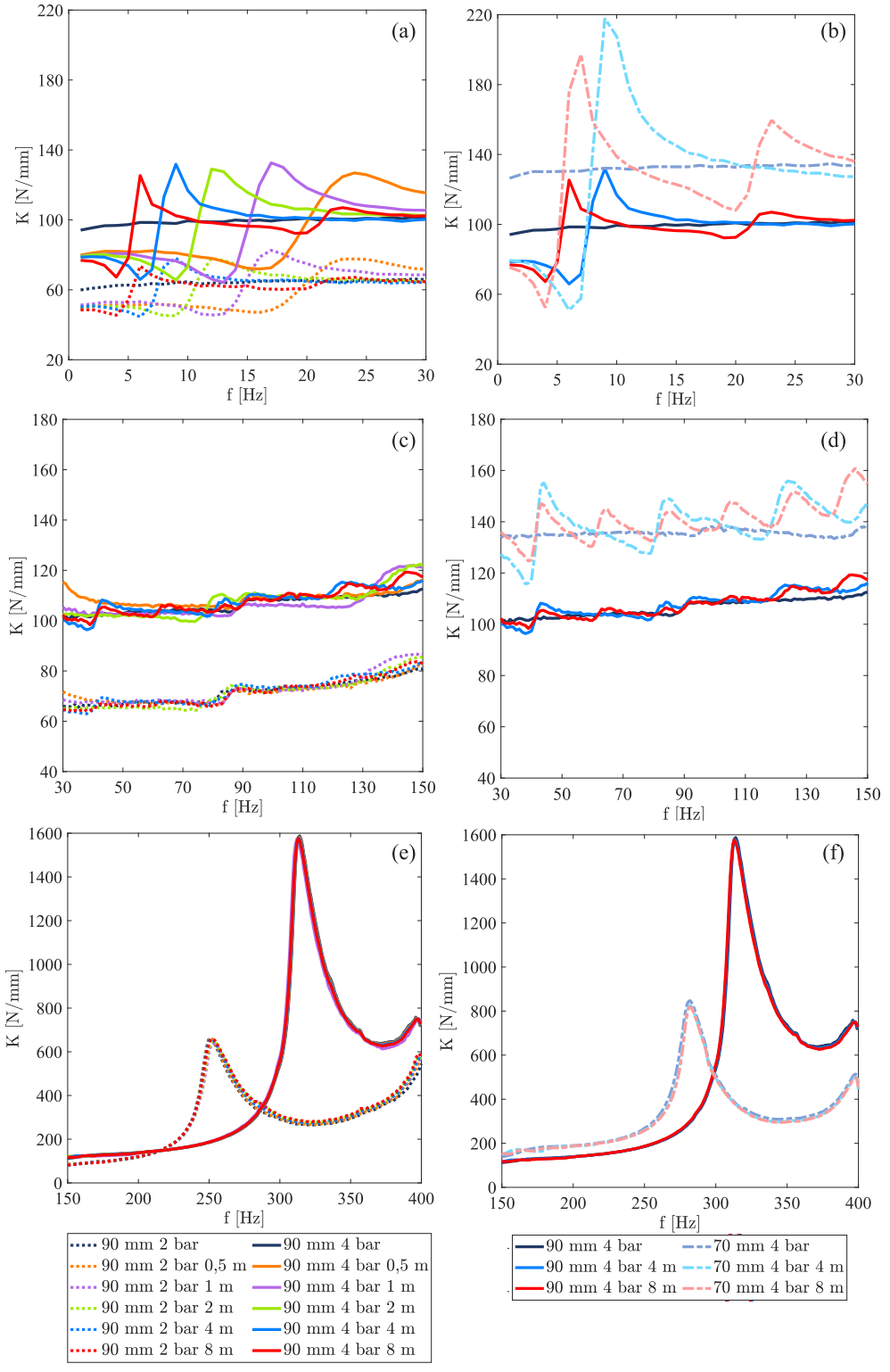

Fig. 4. Experimental dynamic stiffness of the pneumatic suspension system for different pipeline lengths (a, c, d) and mounting heights (b, c d) distinguished according to the value frequency *Low* (a, b), *Intermediate* (c, d), *High* (e, f).

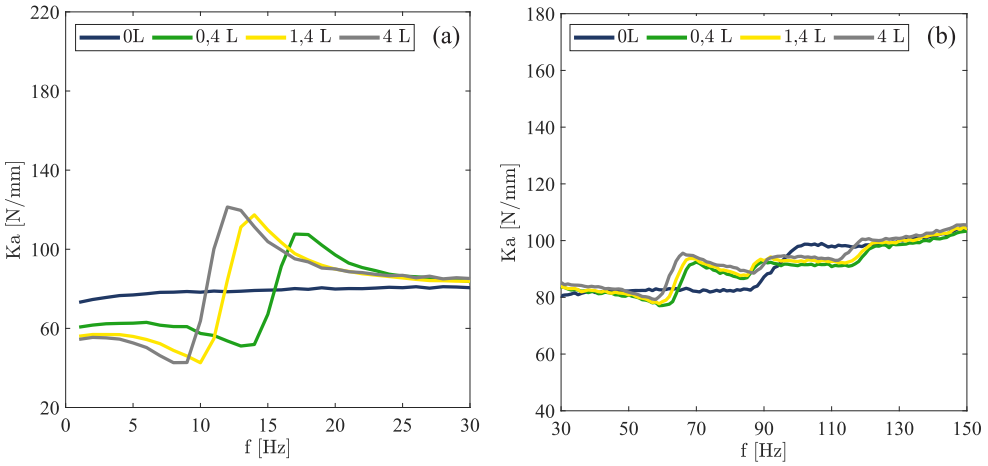

Fig. 5. Experimental dynamic stiffness of the pneumatic suspension system to analyse the reservoir volume in (a) *Low* and (b) *Intermediate* frequencies.

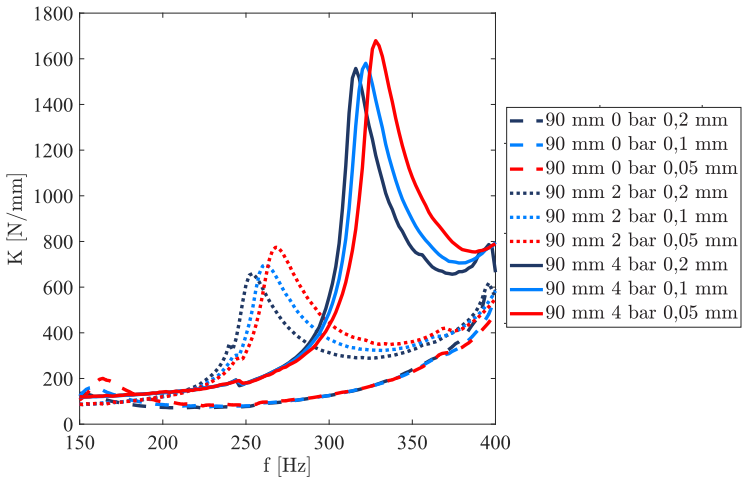

Fig. 6. Experimental dynamic stiffness of the pneumatic suspension system to analyse the excitation amplitude in *High* frequency.

In the present research, ABAQUS software is employed for the modelling of the pneumatic suspension. The methodology employed for the FE modelling of the bellow is based on a previous work [23], enhanced here with the addition of the pipeline and reservoir, considering the non-linear material definition and extending the frequency range of the model up to 400 Hz. The coupling between the internal air pressure and the deformation of the bellows is done though a surface-based *fluid cavity*. The fibres of the composite material of the air spring's diaphragm are incorporated as an embedded uniaxial reinforcement using *rebar* elements. These elements create an equivalent orthotropic layer parallel to the mid-surface of the shell thickness considering the geometry of the fibres (diameter and spacing) oriented at 60° and -60°, where the material of the fibres is defined as linear elastic. The model also includes a non-linear definition of the behaviour of the elastomeric material (more details are given in Section 3.1). Lastly, the fluid exchange between the cavities is governed by a user defined function *VUFLUIDEXCH* coded in FORTRAN (further information can be found in Section 3.2).

3.1. Definition of the non-linear elastic and viscoelastic behaviour of elastomeric material

In order to define the non-linear elastic and non-linear dynamic response of the pneumatic suspension system to quasi-static and harmonic excitations, the non-linear elastic and rate-dependent (viscoelastic) material properties of the elastomeric material must be considered. In finite element models, the mechanical properties of the materials are defined through material models. These are semi-empirical equations in which material behaviour is described using parameters that need to be identified by fitting the model to the behaviour of the material as measured from tests on specimen. As the complexity of the model increases, more parameters need to be included in the model, and model calibration becomes increasingly challenging. The specific characteristics or rubber material that are taken into account in the present work are the non-linear elasticity and the frequency or rate-dependence.

Most finite element codes consider the possibility of including quite directly these material definitions, by the use of hyperelastic models (in order to consider non-linear elastic behaviour) and linear viscoelastic models (in order to implement frequency dependent behaviour of the elastomeric material), respectively. However, modelling the effect of the dynamic behaviour of the elastomeric material on excitation amplitude is not as straightforward and requires more complicated models to be implemented [27]. They include parallel networks representing the elastic, viscoelastic (rate-dependence) and friction (amplitude-dependence) phenomena.

In this work, the quasi-static hyperelastic behaviour of the rubber material is defined according to the Yeoh model for nearly incompressible materials [28] This model is based on a phenomenological strain energy function (U) defined as a cubic function of the first invariant I_1 of the stress tensor:

$$U = C_{10}\left(I_1 - 3\right) + C_{20}\left(I_1 - 3\right)^2 + C_{30}\left(I_1 - 3\right)^3, \tag{2}$$

where C_{10}, C_{20}, C_{30} are the parameters of the model.

The rate-dependent behaviour of the bellows material is represented in the frequency domain using a Prony series representation in which the shear modulus is defined as the sum of a constant term representing the long-term (i.e. quasi-static) value of the modulus and N visco-elastic contributions described as Maxwell elements (viscous dashpot with serial stiffness) [29].

The complex-valued, frequency dependent shear modulus of the material is defined as:

$$G(\omega) = G_s(\omega) + iG_\ell(\omega), \tag{3}$$

$$G_s(\omega) = G_0\left[1 - \sum_{i=1}^{N} \bar{g}_i^P\right] + G_0 \sum_{i=1}^{N} \frac{\bar{g}_i^P \tau_i^2 \omega^2}{1 + \tau_i^2 \omega^2} \quad ; \quad G_\ell(\omega) = G_0 \sum_{i=1}^{N} \frac{\bar{g}_i^P \tau_i \omega}{1 + \tau_i^2 \omega^2}. \tag{4}$$

$$G_\infty = G_O\left[1 - \sum_{i=1}^{N} \bar{g}_i^P\right],$$

with i the imaginary unit, $G_s(\omega)$ the storage modulus and $G_\ell(\omega)$ the loss modulus, the two components of the modulus being expressed as [30]:

$$G_s(\omega) = G_0\left[1 - \sum_{i=1}^{N} \bar{g}_i^P\right] + G_0 \sum_{i=1}^{N} \frac{\bar{g}_i^P \tau_i^2 \omega^2}{1 + \tau_i^2 \omega^2} \quad ; \quad G_\ell(\omega) = G_0 \sum_{i=1}^{N} \frac{\bar{g}_i^P \tau_i \omega}{1 + \tau_i^2 \omega^2}. \tag{5}$$

In Eq. (5) G_0, $\bar{g}_i^P$ and τ_i^2 are the parameters of the Prony series. Parameter G_0 is the initial shear modulus when the material is subjected to a step change of the shear strain, and is related to the long-term shear modulus G_∞ by the relationship:

$$G_\infty = G_O\left[1 - \sum_{i=1}^{N} \bar{g}_i^P\right],$$

whilst parameters $\bar{g}_i^P$ and τ_i^2 are respectively the non-dimensional shear modula and the time constants of the N Maxwell elements.

In order to identify the parameters of the elastomer material model, two kinds of tests material characterisation are performed using an Instron 4467 and an Instron MHF 25 testing machines. Quasi-static tension [31], compression [32] and simple shear [33] tests are performed on specimens, following the procedure stated in the standards, in order to obtain the non-linear elastic behaviour of the material and the parameters of the hyperelastic model. Fig. 7 shows the set up of a compression, traction and simple shear specimens. Fig. 8 compares the stress–strain curves from the experimental tests with the predictions of the Yeoh model implemented in the FEM model: a very good agreement is observed between the two series of data.

A dynamic DMA (Dynamical mechanic analysis) frequency sweep is conducted in simple shear [34] to determine the frequency or time-dependent storage and loss modulus and adjust the $\bar{g}_i^P$ and τ_i coefficients for each term in the Prony series.

It is worth remarking that the implemented material model does not consider the influence of the harmonic excitation amplitude on the response when Frequency Response Functions are to be calculated. Yeoh's hyperelastic model accounts for the non-linear elastic behaviour neglecting frequency dependence effects, whereas the Prony series aims at reproducing the frequency dependence of the material disregarding the influence of the amplitude. Based on the experimental results shown in Fig. 9, this is a good approximation when elastomers are relatively soft (the trend is almost insensitive to the amplitude of deformation for NR50 in Fig. 9b) but could lead to errors if more heavily filled elastomers are used, see the trend with amplitude for material NR70 in Fig. 9b. As the air spring being modelled in this work is manufactured with a soft Shore A 50 natural rubber, the material model adopted is acceptable.

3.2. Model of the pneumatic system

The air spring and the reservoir of the pneumatic system are represented in the FE model in ABAQUS by filled surface pneumatic cavity elements, in which a membrane defines the cavity boundaries sharing the nodes with the structural elements and allowing the calculation of the pressure inside the cavity and the volume of the cavity.

The air inside the two cavities is modelled as an ideal gas with molecular weight 0.0289 kg/mol, in which all heat transformations are assumed to be polytropic. The heat capacity is defined via the Shomate equation with coefficients a = 28.11, b = 1.967e−3, c = 4.802e−6, d = −1.966e−9 and e = 0 in the SI units and for a temperature range of 273-1800K [35]. Since the finite element

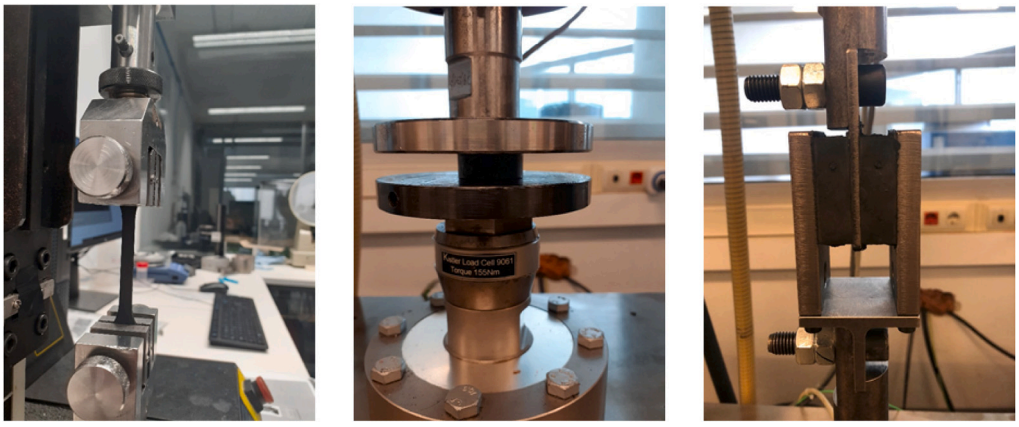

Fig. 7. Set-up of rubber material characterisation tests: (a) Tension test, (b) Compression test, (c) Simple shear test.

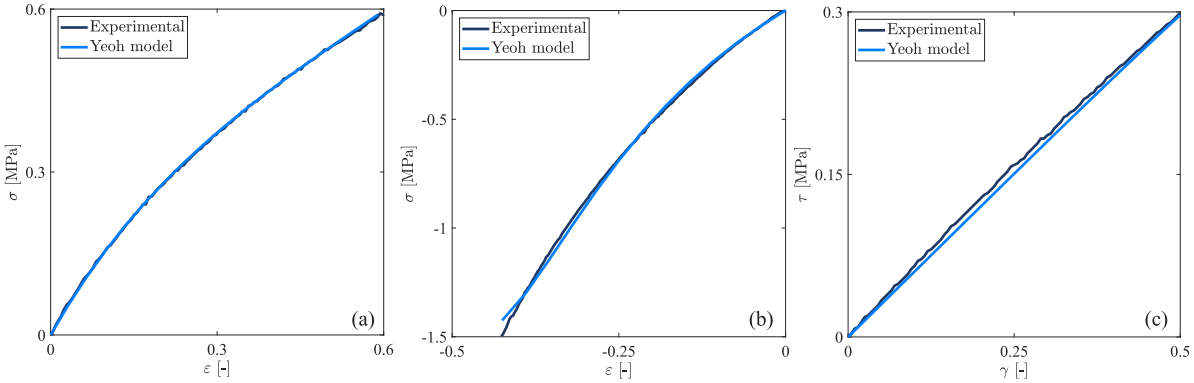

Fig. 8. Stress-strain relation of the rubberlike material: (a) tension, (b) compression and (c) shear tests.

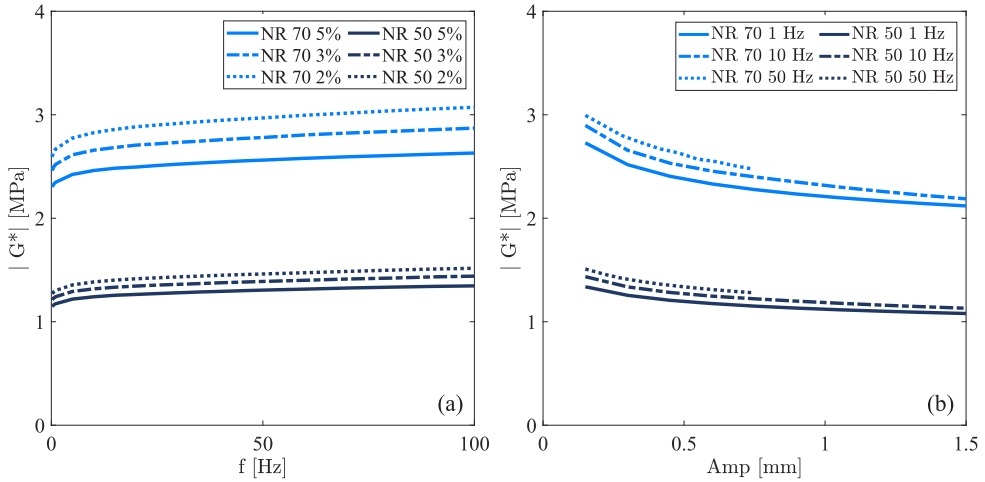

Fig. 9. Modulus of the dynamic stiffness for a shear DMA test of two hardness natural rubbers, referenced as NR50 (soft rubber) and NR70 (stiff rubber): (a) for different excitation amplitudes, (b) for different excitation frequencies.

model is solved in an explicit way, the heat exchange between the system and the surrounding environment allows the definition of a generic polytropic index, corresponding to a transformation which is neither isothermal nor adiabatic.

The unknown values of air pressure in the two cavities are considered as two additional degrees of freedom of the FEM model, each one associated to the reference node of the corresponding cavity. These reference nodes are used to define the air flow in the pipe connecting the two cavities. However, in ABAQUS no model is directly available for the pipe connecting the two air volumes. Therefore, a *fluid exchange* linking element is used, which defines the mass flow rate of the air in the pipe ($\dot{m}$) as a function of the pressure difference between the two cavities ($\Delta p_{br} = p_b - p_r$).

This fluid exchange linking element can be defined in the form of a lookup table or as a user defined function. The first option assumes that the amplitude of the dynamic excitation is sufficiently small so that the fluid equations can be linearised around the quasi-static state of the fluid. In this way, however, it is impossible to describe the internal dynamics of the air inside the pipeline. That is why, in the present work the mass flow rate is defined using a VUFLUIDEXCH user-defined subroutine [36].

The user-defined routine assumes the air in the pipe behaves as a viscous incompressible fluid performing a mono-dimensional sub-sonic flow. Under these assumptions, air velocity in the pipe (u_p) is obtained using the following first-order, non-linear differential equation [12]:

$$\rho_p L_p \frac{du_p}{dt} = p_b - p_r - \frac{32\mu L_\mathrm{P}}{D_\mathrm{P}^2} u_p - \frac{1}{2} l_\mathrm{p} \rho_p \left|u_p\right| u_p, \tag{6}$$

where L_p and D_p are the length and diameter of the pipe, p_b and p_r are the pressures of the air spring and reservoir, ρ_p is air density in the pipe, μ is the dynamic viscosity of the air and l_p are the local losses in the pipe due to singularities and friction losses derived from the Darcy formula.

Air density inside the pipe is defined as the average of air density in the bellows and in the surge reservoir, respectively ρ_b and ρ_r:

$$\rho_p = \frac{\rho_b + \rho_r}{2} = \frac{1}{2}\left(\frac{p_b}{RT_b} + \frac{p_r}{RT_r}\right), \tag{7}$$

The mass flow rate in the pipe is defined as:

$$\dot{m} = \rho_p A_p u_p, \tag{8}$$

with A_p the area of the cross-section of the pipe. Eqs. (6)–(8) altogether define the fluid exchange linking element. This set of equations is solved in the user-defined routine using Euler's explicit method.

It is worth noting that although most models proposed in the literature idealise the air as an incompressible fluid under the assumption of adiabatic transformations [12,13,20], Docquier [37] remarks the importance of considering the compressibility of the air towards model accuracy. The proposed enhanced FEM includes the compressible behaviour of the air and the polytropic heat exchange.

4. Results

4.1. Static results

In this section, the results of quasi-static tests are compared to the outputs of the FEM model described in Section 3 in terms of the static stiffness of the air spring, defined as the real-valued ratio of the increment in the force produced by the spring over the change of the working height, starting from a reference condition defined by a reference height and air pressure inside the spring. These results are also compared to an estimate of the static stiffness obtained from an analytical model of the static airspring behaviour described below.

The ability of an air spring to support an axial load F depends on its effective area (A_e) and on the air pressure (p), which both depend in turn on the vertical deflection of the bellows (z). Often the inherent structural force of the composite bellows (F_b) is neglected [13,37] but, for the air spring considered here, this term cannot be neglected due to the small and relatively stiff construction of the bellows [20]. Therefore, the static axial force produced by the spring can be written as:

$$F = p(z)A_e(p,z) + F_b(z), \tag{9}$$

Assuming small values of the deflection z, this equation can be linearised in the neighbourhood of a reference state, providing the following analytical expression of the air spring stiffness K:

$$K = \frac{\mathrm{d}F}{\mathrm{d}z} = p_0 \left|\frac{\partial A_e}{\partial p}\right|_{z_0,p_0} \frac{\mathrm{d}p}{dz} + p_0 \left|\frac{\partial A_e}{\partial z}\right|_{z_0,p_0} + A_e(p_0,z_0)\frac{\mathrm{d}p}{dz} + \frac{\mathrm{d}F_b}{dz}, \tag{10}$$

where z_0 and p_0 are the values of deflection and air pressure in the reference state. The effective area and its gradients with respect to pressure p and deflection z are obtained from manufacturer data, whilst the structural stiffness is experimentally measured. Frequently, it is assumed that the stiffness due to the effective area gradient only depends on the air spring height [13,37], but in small bellows the term related to the gradient of the effective area with respect to pressure $\frac{\partial A_e}{\partial p}$ is not negligible. Moreover, the gradient of air spring pressure with respect to air spring deflection $\frac{\mathrm{d}p}{\mathrm{d}z}$ is important in small bellows like the one considered here, compared to larger ones often employed, for instance, in railway vehicles. This term can be expressed based on a state equation

Table 3
Comparison of the static stiffness between experimental tests (EXP), FEM model (FEM) and mathematical equation (Math) for nominal height of 90 mm of the air spring and without reservoir.

p_0 (bar)	EXP (N/mm)	FEM (N/mm)	Deviation$_{FEM}$ (%)	Math (N/mm)	Deviation$_{Math}$ (%)
2	43.0	43.1	0.2	43.7	1.6
3	62.4	64.7	3.7	61.8	−1
4	77.7	76.7	−1.3	78.9	1.5
5	94.2	100.1	6.3	95.5	1.5

describing the evolution of the thermodynamic state for the air in the air spring: since the compression of the bellows changes the internal volume of the air spring and affects both air pressure and temperature, the process can be described as polytropic with generic index n:

$$pV^n = p_0 V_0^n. \tag{11}$$

Taking the derivative of Eq. (11) with respect to deflection z:

$$\frac{\mathrm{d}p}{\mathrm{d}z} V_0^n + n p_0 V_0^{n-1} \frac{\mathrm{d}V}{\mathrm{d}z} = 0,$$

the gradient of air spring pressure with respect to air spring deflection is obtained as:

$$\frac{\mathrm{d}p}{\mathrm{d}z} = -n \frac{p_0}{V_0} \frac{\mathrm{d}V}{\mathrm{d}z}. \tag{12}$$

Introducing Eq. (12) in Eq. (10) and using data from the manufacturer for the effective area and its gradients, an analytical expression of the static air spring stiffness is obtained for a given reference state described by working height z_0 and pressure p_0.

The polytropic index n is determined by the amount of heat exchanged with the surrounding environment: in case the deformation of the air spring occurs over a sufficiently long time, the heat generated by air compression is fully transferred to the surrounding environment and the process can be well approximated as being isothermal, $n = 1$. If otherwise the deformation of the spring takes place over a relatively short time, heat exchange with the environment is limited and the process can be approximated as being adiabatic, so the polytropic index n can be set to the specific heat ratio coefficient γ. Usually, in a low frequency range and particularly under quasi-static conditions, the air spring deformation process is assumed to be isothermal whereas at higher frequencies the adiabatic assumption is used [37–39]. Pintado et al. performed experimental tests aimed at identifying the polytropic index and found values close to 1 (isothermal) in the 0.1–1 Hz frequency range [40]. However, it should be noted that in this paper a much wider frequency range, up to hundreds of Hz is addressed, so the results from [40] cannot be directly applied to the models presented here. It should also be noted that Pintado et al. found different values of the polytropic index depending on the method used to process their measurements to derive an estimate of the polytropic index, see Figs. 6 and 8 in their paper. In the present work, air transformation process in the air spring is assumed to be polytropic in the FEM model and isothermal when Eq. (12) is used.

Table 3 compares the measured static stiffness of the air spring (column "EXP"), the value obtained from the Finite Element (FE) model described in Section 3 (column "FEM") and the value obtained from Eqs. (10) and (12) (column "Math"), for different values of the pressure in the reference state p_0 and considering the air spring not connected to a surge reservoir. The results provided by the FE model and by the analytical expression are both in good agreement with the measured values, with deviations below 7% in all cases and below 4% in most cases. An extended comparison of the stiffness values provided by the two models with the measured stiffness is provided in Fig. 10 for different values of the ratio of the volume of the reservoir V_r over the volume of the bellows V_b. Also in this case, a very good agreement is observed.

4.2. Dynamic results

Fig. 11 gives an overview of the dynamic stiffness of the air spring mounted in the nominal height with a reservoir of 0.4 l and a connecting pipe of 4 m. The proposed model accurately predicts the resonance frequencies of the suspension falling in the *low* and *high* frequency ranges, and also provides an accurate prediction of the amplitude of the corresponding resonance peaks, with deviations from the measured values below 6% and below 9% for the low and high frequency ranges respectively. However, the detail of the diagram in the *intermediate* frequency range (30 to 150 Hz) shows that the model misses to reproduce the measurements in terms of the small-amplitude resonance peaks taking place in this frequency range, which are due to the effect of standing waves in the pipe, as further discussed in Section 4.2.2.

4.2.1. Results for the Low frequency range

The predictions of the FEM model for *low* frequency peaks have been compared to the experimental data and to the results obtained from implementing the set of differential equations provided by Facchinetti et Al. [12] into the analysed small pneumatic system. This last approach is denoted as the dynamic thermodynamic model.

As shown in Fig. 12, both models are able to predict the first resonance peak, which is due to air's inertia in the auxiliary volume (reservoir and pipeline). As summarised in Table 4, the frequency value is reproduced with very good accuracy, however,

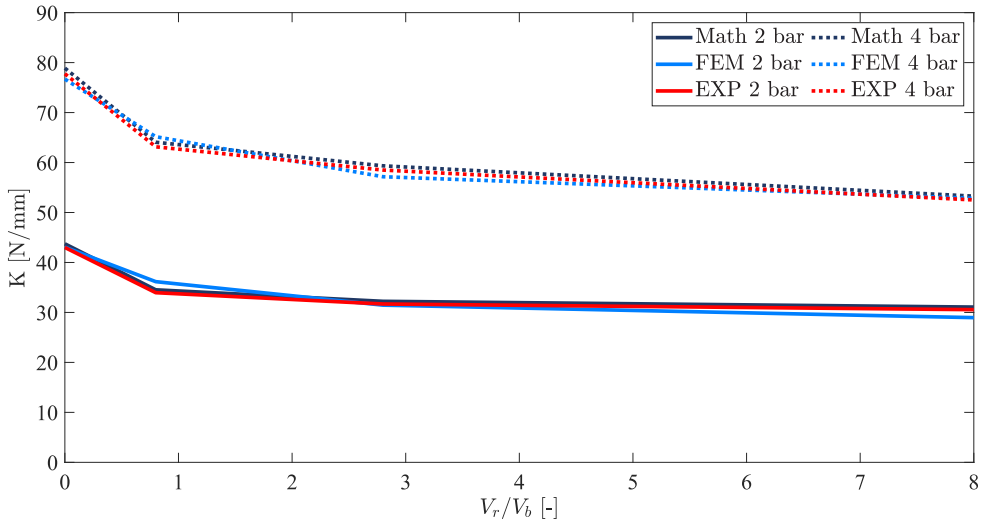

Fig. 10. Volume relation influence in the stiffness of the pneumatic system for a nominal height of the air spring of 90 mm.

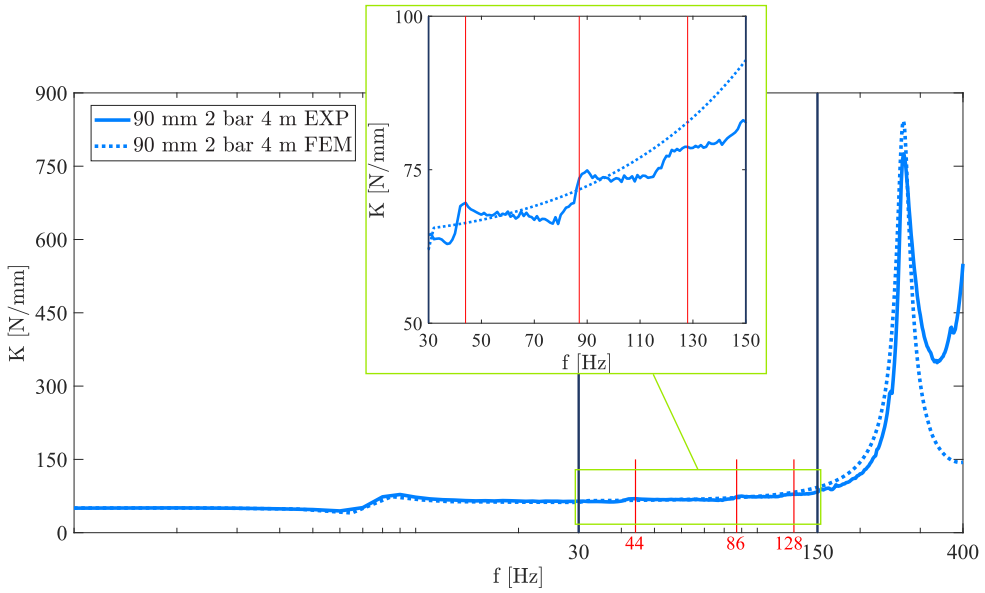

Fig. 11. Comparison between the experimental and simulated dynamic stiffness of the pneumatic suspension system.

the dynamic stiffness value at resonance is predicted by the two models to a slightly lower accuracy, with errors always below 9% and mostly below 6%. The frequency sample for the experimental tests and the mathematical approach is 1 Hz, whereas it is 0.5 Hz for the FEM model. The presence of an anti-resonance of the dynamic stiffness is also clearly visible in the experimental results shown in Fig. 12 and is well reproduced by the FEM model, whereas it is reproduced to a lesser degree of accuracy by the thermodynamic model. This is due to the fact that the FEM model considers the frequency-dependent behaviour of the rubber-like material of the bellows and also describes state transformations in the air inside the suspension as a general polytropic process, whereas the thermodynamic model neglects the frequency-dependent behaviour of the bellows and approximates heat transformations to adiabatic.

4.2.2. Results for the Intermediate frequency range

The resonance peaks observed in this frequency range are due to the formation of standing waves in the air inside the pipe. Fig. 13 illustrates this phenomenon: the standing wave (Δp) is considered as the interference of two harmonic pressure waves Δp_b and Δp_r) having the same amplitude (p_{max}) and wavelength (λ), which are reflected at both ends of the pipeline. The ends of the pipeline are the bellows to one side and the reservoir to the other side.

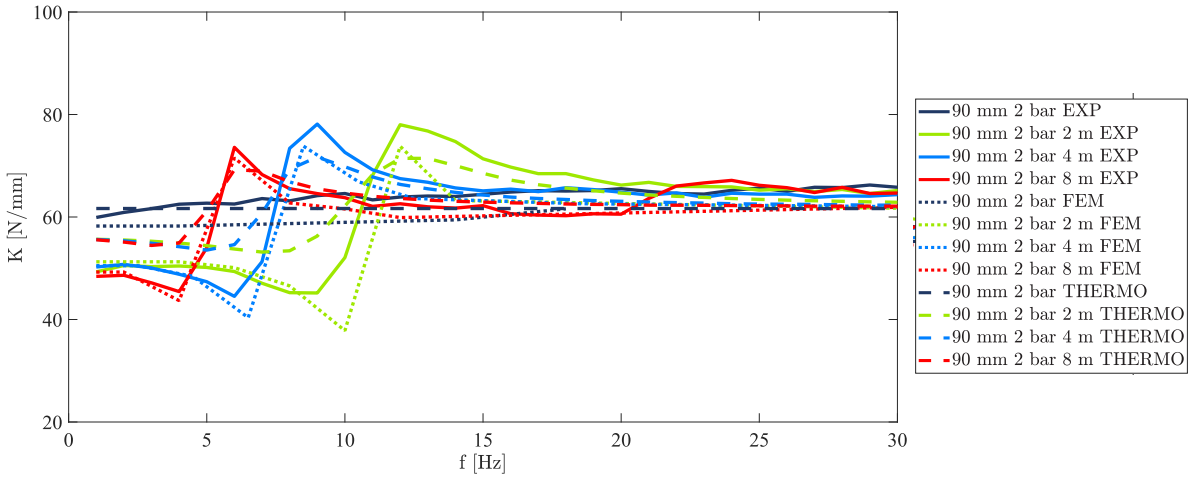

Fig. 12. Comparison between experimental and simulated pneumatic system performance for low frequency range and 2 bar pressure.

Table 4
Comparison of the low resonance frequency between experimental (Exp), mathematical (Math) and FEM models for nominal height of 90 mm of the air spring with reservoir for different pipeline lengths and reference pressure P_0 = 2 bar.

Resonance frequency (Hz)					
L_p (m)	Exp (Hz)	Math (Hz)	Deviation$_{Math}$ (%)	FEM (Hz)	Deviation$_{FEM}$ (%)
2	12.0	12.0	0.0	12.0	0.0
4	9.0	9.0	0.0	8.5	−6.0
8	6.0	6.0	0.0	6.0	0.0
Dynamic stiffness in resonance condition (N/mm)					
L_p (m)	Exp (N/mm)	Math (N/mm)	Deviation$_{Math}$ (%)	FEM (N/mm)	Deviation$_{FEM}$ (%)
2	73.6	69.2	−6	71.5	−2.8
4	78.4	71.7	−8.2	73.8	−5.5
8	78	71.45	−8.4	73.8	−5.4

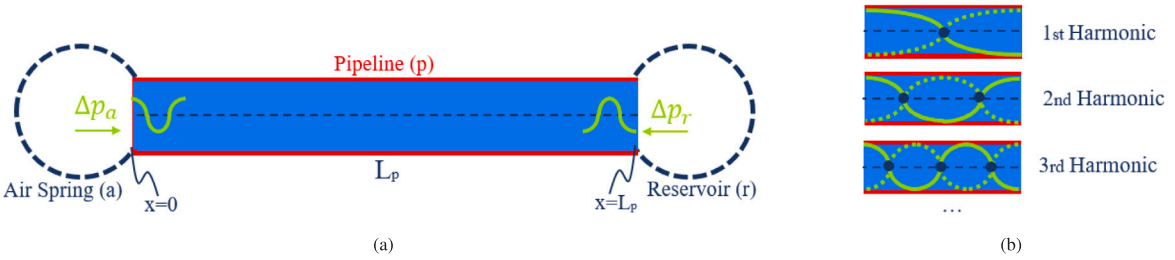

Fig. 13. Layout of the modelling of the pipeline in medium frequency: (a) summary outline and (b) wave shape.

Air pressure in the pipe is governed by the classic partial derivative differential equation describing the propagation of a pressure perturbation in a one-dimensional domain [41]. The solution of this equation is the sum of two pressure waves Δp_b and Δp_r moving across the pipe in opposite directions:

$$\begin{aligned} \Delta p_b(x,t) &= p_{max} sin(\frac{2\pi x}{\lambda} + wt) \\ \Delta p_r(x,t) &= p_{max} sin(\frac{2\pi x}{\lambda} - wt). \end{aligned} \tag{13}$$

The superimposition of the two travelling waves is a standing wave in the form:

$$\Delta p(x,t) = \Delta p_b + \Delta p_r = 2p_{max} sin(\frac{2\pi x}{\lambda}) cos(wt). \tag{14}$$

Table 5
Intermediate resonance frequencies, from the stationary wave equation Eq. (16) (Wave Eq.) and from the experimental results results (EXP).

Length (m)	EXP (Hz)	Wave Eq. (Hz)	Error (%)
2	84 - 146	84 - 158	0 - 8
4	43 - 84 - 126 - 146	44 - 86 - 128 - 170	2 - 2 - 2 - 16
8	23 - 43 - 64 - 84 - 105	23 - 44 - 65 - 86 - 107	0 - 2 - 2 - 2 - 2

As the pipeline connects two relatively large air volumes at its extremities, i.e. the bellows and the reservoir, the spatial gradient of air pressure takes zero value at both ends of the pipe:

$$\left|\frac{\partial \Delta p}{\partial x}\right|_b = \left|\frac{\partial \Delta p}{\partial x}\right|_r = 0.$$

Considering the above boundary conditions, the wavelengths λ_k of the pressure standing waves that can be established in the pipe are obtained as the integer sub-multiples of the length of the pipe L_p:

$$\lambda_k = \frac{2L_p}{k} \tag{15}$$

with k the harmonic number of the standing wave. Fig. 13b shows the shape of the standing wave for the three lowest values of the harmonic number.

As the wavelength can be written as the speed of sound (V_s) divided by the frequency, the resonance frequencies for a pipeline having length (L_p), and therefore the resonance frequencies of the pneumatic system in the *Intermediate* frequency range ($w_{k,int}$), can be calculated as:

$$w_{k,int} = 2\pi \frac{kV_s}{2L_p}. \tag{16}$$

Table 5 shows that this equation provides a good prediction of the resonance frequencies found from the measured dynamic stiffness of the pneumatic suspension, with errors below 2% except for the mode corresponding to the experimental value of 146 Hz for pipe length 4 m, where the error is 16%. It should be noted however that Eq. (16) only provides information about the resonance frequency, whilst the peak value of the dynamic stiffness should be derived from a more complex model which is a topic for a future extension of this work. Nevertheless, comparing the resonance peak amplitude of these intermediate peaks with the ones in low and high frequencies (see Fig. 3), for the given application, they are found to have very small effect on the dynamic behaviour of the suspension.

However, this resonance effect can be significant in other types of air springs. Mendia-Garcia et al. [23] states, for instance, that the first vibration modes of a rolling lobe bellows employed in railway vehicles occur below 100 Hz, and may overlap with resonances from the standing waves in the pipe, which would then have a significant effect on the overall dynamic behaviour of the pneumatic suspension in the intermediate and high frequency ranges.

4.2.3. Results for the High frequency range

Lastly, Fig. 14 shows the comparison between the measured dynamic stiffness in the *High* frequency range (from 150 to 400 Hz) and the predictions from the FEM model. The FEM model accurately predicts the FRF of the air spring for different values of the nominal pressure. The model captures the effects on the dynamic stiffness of the suspension caused by the first vertical structural vibration mode of the air spring. The modal shape of this vibration mode is also shown in Fig. 14. It should be noted that in the FEM model, the reinforced rubber-like composite material is defined as a hyperelastic and linear viscoelastic material. Therefore, the FEM model cannot capture the dependence of the dynamic stiffness on the amplitude of height variation applied.

In addition, the validated FEM model can also predict the frequency and modal shape of additional vibration modes in any direction, not only the axial or vertical modes. For instance, Table 6 summarises the first six modes of the system for different values of the reference pressure. Unfortunately, since the measurements are obtained from a pure axial excitation, the effect of these additional resonances is not visible in the measured dynamic stiffness, so it is not possible to compare these predictions from the FEM model with corresponding experimental data. According to the results from the FEM model, the considered air spring has at least 48, 23 and 17 vibration modes below 1000 Hz for inner pressure of 0, 2 and 4 bar, respectively.

5. Conclusions

In this paper, the dynamic performance of a pneumatic suspension consisting of an air spring connected via a pipeline to a surge reservoir is experimentally analysed and simulated by means of an enhanced FEM model and simplified analytical models. The present study extends significantly previous experimental and modelling investigations of pneumatic suspensions which, to the best knowledge of the authors, were mostly confined to a frequency range up to 30–40 Hz, whereas the frequency range addressed in this work is up to 400 Hz, thus covering the entire frequency range which is relevant to structure-borne vibration transmission. By extending the frequency range addressed, the existence of new resonances is found and their relationship to the physical parameters of the pneumatic suspension is explained. Furthermore, the proposed modelling approach provides results that are in very good

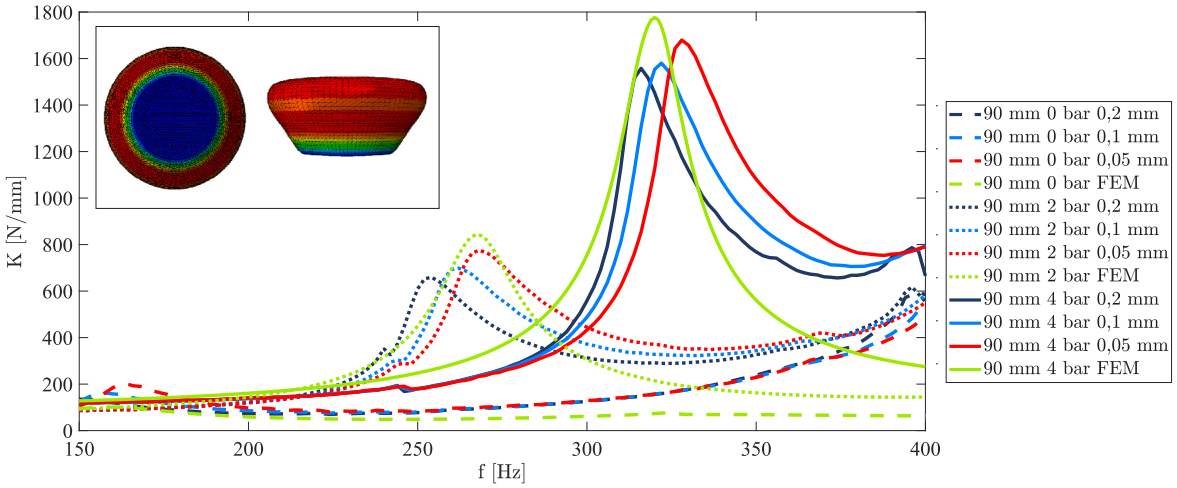

Fig. 14. Comparison between experimental and simulated air spring alone frequency response function.

Table 6
Eigenfrequencies and vibration modes of the air spring as predicted by the FEM model for different values of the reference pressure.

	Eigenfrequency (Hz)			
mode	0 (bar)	2 (bar)	4 (bar)	shape
1	159	268	320	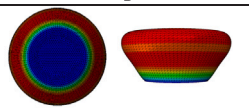
2	291	374	414	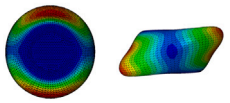
3	301	524	629	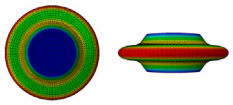
4	308	525	627	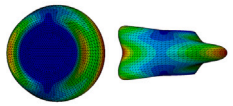
5	331	534	630	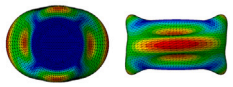
6	382	564	653	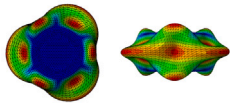

quantitative agreement to the experiments in terms of the resonance frequencies and values of the dynamic stiffness of the suspension at different resonances.

Based on a comprehensive experimental characterisation of the air spring suspension, the resonances of the suspension are categorised as belonging to three distinct frequency ranges: *low frequency* (0–30 Hz), *intermediate frequency* (30-150 Hz), *high frequency* (beyond 150 Hz), where the major conclusions drawn from this study are:

- *low frequency*: in this frequency range one single resonance is found, which is due to the motion of air as an incompressible fluid in the pipe connecting the bellows to the reservoir. This resonance is also found using other models available in the literature [6,8–17] but the FEM model presented in this work allows a more accurate prediction of the anti-resonance taking

place at a frequency slightly lower than the resonance, see Fig. 12. Regarding the effect of system parameters, the single resonance frequency found in the low-frequency range is decreasing with increasing volume of the surge reservoir whilst a change in the reference pressure does not affect the resonance frequency but increases the overall stiffness of the suspension. In addition, the resonance frequency is slightly affected by the nominal working height of the air spring, with smaller height values producing higher values of the natural frequency.

- *intermediate frequency*: the resonances experimentally observed in this frequency range are related to the formation of standing waves in the pipe. The values of these natural frequencies are well predicted by a simple formula based on the relationship between the frequency and wavelength of the standing waves. Therefore, the only design parameter of the pneumatic suspension affecting these resonance frequencies is the length of the pipeline. Smaller mounting heights slightly amplify the amplitude of the resonance peaks.
- *high frequency*: the resonances taking place in this frequency range are related to the structural dynamic behaviour of the bellows. One single vibration mode, namely the first vertical mode of the bellows, mainly affects the dynamic stiffness of the suspension in the frequency range up to 400 Hz. The dynamic stiffness and the modal shape of the vibration modes are predictable with the FEM model. Both these quantities are highly dependent on the structural and material properties of the bellows. It should be noted that the elastomer material model considered in this work does not include non-linear viscoelasticity and, thus, the small differences found in the dynamic stiffness measured at different amplitudes of excitation are not reproduced by the FEM model.

This paper contributes to the further understanding of the dynamic behaviour of an air spring with a reservoir connected by a pipe. The proposed methodology can be applied in the design stage of pneumatic suspensions by choosing the geometry, materials, pipeline, and reservoir that provide the desired dynamic response for the intended application, covering a frequency range not addressed by previously published models.

CRediT authorship contribution statement

I. Mendia-Garcia: Conceptualization, Methodology, Validation, Formal analysis, Investigation, Writing – original draft. **A. Facchinetti:** Conceptualization, Methodology, Writing – review & editing, Supervision. **S. Bruni:** Conceptualization, Writing – review & editing, Visualization, Supervision. **N. Gil-Negrete:** Conceptualization, Writing – review & editing, Supervision.

Declaration of competing interest

The authors declare that they have no known competing financial interests or personal relationships that could have appeared to influence the work reported in this paper.

Data availability

No data was used for the research described in the article.

Acknowledgements

The authors are grateful for the financial support for international mobility of Fundación Bancaria “La Caixa”, Spain.

References

[1] M.W. Holtz, J. Van Niekerk, Modelling and design of a novel air-spring for a suspension seat, J. Sound Vib. 329 (21) (2010) 4354–4366.
[2] S. Bruni, J. Vinolas, M. Berg, O. Polach, S. Stichel, Modelling of suspension components in a rail vehicle dynamics context, Veh. Syst. Dyn. 49 (7) (2011) 1021–1072.
[3] N.Y.P. Vo, T.D. Le, Adaptive pneumatic vibration isolation platform, Mech. Syst. Signal Process. 133 (2019) 106258.
[4] Y. Zheng, W.B. Shangguan, S. Rakheja, Modeling and performance analysis of convoluted air springs as a function of the number of bellows, Mech. Syst. Signal Process. 159 (2021) 107858.
[5] S. Kandasamy, B. Nicolsen, A.A. Shabana, G. Falcone, Evaluation of effectiveness of pneumatic suspensions: Application to liquid sloshing problems, J. Sound Vib. 514 (2021) 116328.
[6] N. Docquier, P. Fisette, H. Jeanmart, Multiphysic modelling of railway vehicles equipped with pneumatic suspensions, Veh. Syst. Dyn. 45 (6) (2007) 505–524.
[7] L. Mazzola, M. Berg, Secondary suspension of railway vehicles-air spring modelling: Performance and critical issues, Proc. Inst. Mech. Eng. F 228 (3) (2014) 225–241.
[8] N. Oda, S. Nishimura, Vibration of air suspension bogies and their design, Bull. JSME 13 (55) (1970) 43–50.
[9] M. Berg, A three–dimensional air spring model with friction and orifice damping, Veh. Syst. Dyn. 33 (sup1) (1999) 528–539.
[10] Vampire, Vampire Pro V6.30 Help Manual, DeltaRail Group Ltd, Derby, 2014, Manual.
[11] A. Alonso, J.G. Gimenez, J. Nieto, J. Vinolas, Air suspension characterisation and effectiveness of a variable area orifice, Veh. Syst. Dyn. 48 (S1) (2010) 271–286.
[12] A. Facchinetti, L. Mazzola, S. Alfi, S. Bruni, Mathematical modelling of the secondary air spring suspension in railway vehicles and its effect on safety and ride comfort, Veh. Syst. Dyn. 48 (S1) (2010) 429–449.
[13] G. Quaglia, M. Sorli, Air suspension dimensionless analysis and design procedure, Veh. Syst. Dyn. 35 (6) (2001) 443–475.

[14] H. Zhu, J. Yang, Y. Zhang, X. Feng, A novel air spring dynamic model with pneumatic thermodynamics, effective friction and viscoelastic damping, J. Sound Vib. 408 (2017) 87–104.
[15] A.J. Nieto, A.L. Morales, A. Gonzalez, J.M. Chicharro, P. Pintado, An analytical model of pneumatic suspensions based on an experimental characterization, J. Sound Vib. 313 (1–2) (2008) 290–307.
[16] H.X. Gao, M.R. Chi, M.H. Zhu, P.B. Wu, Study on different connection types of air spring, in: In Applied Mechanics and Materials, Vol. 423, Trans Tech Publications Ltd., 2013, pp. 2026–2034.
[17] Y. Zheng, W.B. Shangguan, S. Rakheja, Modeling and analysis of time-domain nonlinear characteristics of air spring with an auxiliary chamber, Mech. Syst. Signal Process. 176 (2022) 109161.
[18] K. Toyofuku, C. Yamada, T. Kagawa, T. Fujita, Study on dynamic characteristic analysis of air spring with auxiliary chamber, JSAE Rev. 20 (3) (1999) 349–355.
[19] H. Sayyaadi, N. Shokouhi, Effects of air reservoir volume and connecting pipes' length and diameter on the air spring behavior in rail–Vehicles, Iran. J. Sci. Technol. Trans. B 34 (2010) 499–508.
[20] Y. Zheng, W.B. Shangguan, A combined analytical model for orifice-type and pipe-type air springs with auxiliary chambers in dynamic characteristic prediction, Mech. Syst. Signal Process. 185 (2023) 109830.
[21] N. Gil-Negrete, F.J. Nieto, A. Pradera-Mallabiabarrena, J. Gonzalez-Prada, On the dynamic stiffness of air springs at medium-high frequencies, in: Proceedings of ISMA 2018 - International Conference on Noise and Vibration Engineering and USD 2018 - International Conference on Uncertainty in Structural Dynamics, Leuven (Belgium), 2018, pp. 3567–3579, 2018 Sep 17-19; 2018.
[22] X. Peng, T. Cheng, S. Shi, et al., Studies on modeling a single-bellows air spring and simulating its inherent characteristics, J. Shen. Univ. Sci. Eng. 30 (2) (2013) 167–172.
[23] I. Mendia-Garcia, N. Gil-Negrete, F.J. Nieto, A. Facchinetti, S. Bruni, Analysis of the axial and transversal stiffness of an air spring suspension of a railway vehicle: mathematical modelling and experiments, Int. J. Rail Transp. http://dx.doi.org/10.1080/23248378.2022.2136276.
[24] J.J. Chen, Z.H. Yin, X.J. Yuan, G.Q. Qiu, K.H. Guo, X.L. Wang, A refined stiffness model of rolling lobe air spring with structural parameters and the stiffness characteristics of rubber bellows, Measurement 169 (2021) 108355.
[25] M.Y. Wu, H. Yin, X.B. Li, J.C. Lv, G.Q. Liang, Y.T. Wei, A new dynamic stiffness model with hysteresis of air springs based on thermodynamics, J. Sound Vib. 521 (2022) 116693.
[26] A.D. Nashif, D.I. Jones, J.P. Henderson, Vibration Damping, John Wiley and Sons, New York, 1985.
[27] J. Hurtado, I. Lapczyk, S. Govindarajan, Parallel rheological framework to model non-linear viscoelasticity, permanent set, and mullins effect in elastomers, in: Proceedings of the Constitutive Models for Rubber. Vol. 8, 2013, pp. 95–100.
[28] O.H. Yeoh, Characterization of elastic properties of carbon-black filled rubber vulcanizates, Rubber Chem. Technol. 63 (1990) 792–805.
[29] S. W.Park, R. Schapery, Methods of interconversion between linear viscoelastic material functions. Part I—A numerical method based on prony series, Int. J. Solids Struct. 36 (11) (1999) 1653–1675.
[30] ABAQUS-simulia user assistance 2020, frequency domain viscoelasticity, dassault systèmes, 2020, https://help.3ds.com/2020/english/dssimulia_established/simacaematrefmap/simamat-c-freqvisco.htm{c}ontextscope=all&highlight=viscoelasticity+frequency&id=&analyticsContext=search-result&analyticsSearch=viscoelasticity%20frequency&myapp=false, (accessed 16 2023).
[31] Rubber, Vulcanised Or Thermoplastic. Determination of Tensile Stress–Strain Properties, UNE-ISO 37, International Organization for Standardization (ISO), 2013.
[32] Rubber, Vulcanized Or Thermoplastic. Determination of Compression Stress–Strain Properties, UNE-ISO 7743, International Organization for Standardization (ISO), 2016.
[33] Rubber, Vulcanized Or Thermplastic. Determination of Shear Modulus and Adhesion To Rigid Plates. Quadruple-Shear Methods, UNE-ISO 1827, International Organization for Standardization (ISO), 2021.
[34] Ubber, Vulcanised Or Thermoplastic. Determination of Dynamic Properties. Parte 1, General Guidance: UNE-ISO 4664-1, International Organization for Standardization (ISO), 2011.
[35] J. Van. Wylen, E. Sonntag, C. Borgnakke, Fundamentals of Classical Thermodynamics, Wiley, New York, 1994.
[36] ABAQUS-simulia user assistance 2020, vufluidexch, dassault systèmes, 2020, https://help.3ds.com/2020/english/dssimulia-established/simacaesubrefmap/simasub-c-vufluidexch.htm{c}ontextscope=all&highlight=vufluidexch&id=&analyticsContext=search-result&analyticsSearch=vufluidexch&myapp=false, 2020 (accessed 16 2023).
[37] N. Docquier, Multiphysics Modelling of Multibody Systems–Application To Railway Pneumatic Suspensions [Dissertation], Université catholique de Louvain, Leuven, 2010.
[38] X. Li, Y. Wei, Y. He, Simulation on polytropic process of air springs, Eng. Comput. 33 (7) (2016) 1957–1968.
[39] M.A. Spiroiu, Railway vehicle pneumatic rubber suspension modelling and analysis, J. Mater. Plast. 55 (1) (2018) 24–27.
[40] P. Pintado, C. Ramiro, A.L. Morales, A.J. Nieto, J.M. Chicharro, The dynamic behavior of pneumatic vibration isolators, J. Vib. Control 24 (19) (2018) 4563–4574.
[41] L. Wallace, Interactions between sound waves, J. Acoust. Soc. Am. 34 (8) (1962) 1039, http://dx.doi.org/10.1121/1.1918241.